Operating characteristics and performance improvements of a 500 W traveling-wave thermoacoustic electric generator

Kai Wang, Daming Sun*, Jie Zhang, Ya Xu, Jiang Zou, Ke Wu, Limin Qiu, Zhiyi Huang

Faculty of Engineering, Zhejiang University, Hangzhou 310027, PR China

Abstract

Traveling-wave thermoacoustic electric generator has drawn increasing attention due to its great prospect in energy conversion. In this work, a traveling-wave thermoacoustic electric generator capable of generating about 500 W electric power is studied numerically and experimentally. The performances and the operating characteristics of the system under different working conditions are tested and analyzed. The maximum electric powers can be obtained with electric load resistance around 100 Ω~120 Ω, and the highest thermal-to-electric efficiencies can be achieved at much larger load resistances. The efficiency at low load resistance is relatively small due to the large pressure amplitudes inside the thermoacoustic system, which increases the dissipations. The variation trends of the electric power and the thermal-to-electric efficiency with the load resistance intrinsically result from the changes of the corresponding acoustic impedance of the linear alternators, which determines the output performance of the thermoacoustic engine meanwhile. The distributions of the acoustic power losses are then calculated and firstly illustrated quantitatively. It is shown that the resonator causes most of the acoustic power losses, and the losses in hot heat exchanger, thermal buffer tube, and feedback tube are also significant. The output performance of the system can be improved by increasing the heating temperature and the mean pressure. A maximum electric power of 473.6 W and a highest thermal-to-electric efficiency of 14.5% are achieved experimentally when the mean pressure is 2.48 MPa and the heating temperature is 650 °C. A pair of linear alternators with a larger swept volume and appropriate acoustic impedances is finally designed to couple with the

* Corresponding author. Tel/Fax: +86-571-87952769 (Daming Sun)

E-mail address: sundaming@zju.edu.cn (Daming Sun)

thermoacoustic torus directly. Numerical results show that the maximum electric power can be increased to 718 W and 1005 W when the mean pressures are kept at 2.48 MPa and 3.20 MPa, corresponding to the improvements of 42.6% and 29.4% compared with those of the original system.

Keywords: thermoacoustic; electric generation; linear alternator; acoustic power

1. Introduction

Conventional power generation systems usually need to burn fossil fuels, including coal, gasoline, and natural gas, etc., which have brought in serious environmental problems in the past centuries. Much more attention has currently been drawn to the developments of alternative energy conversion technologies, such as those based on fuel cells [1], photovoltaics [2], thermoacoustics [3], thermoelectrics [4], piezoelectrics [5], and thermomagnetics [6], etc.

Thermoacoustic electric generator (TEG) is among one of the most promising power generation systems, which can be easily scaled to provide an electric power from milliwatts to kilowatts. It typically consists of a thermoacoustic engine and acoustoelectric convertors, such as linear alternators (LAs), piezoelectric transducers, etc. Thermoacoustic engine eliminates mechanical moving components at high temperature region and is only comprised of pipes and several heat exchangers [7-15]. Thus, TEG is much more structurally simple, cost effective, and reliable compared to other mechanical power generation systems at similar power levels, such as Stirling generators, gas turbines, etc. Besides, traveling-wave type TEG [8], which is based on an intrinsic reversible thermodynamic cycle similar to Stirling cycle, is more efficient compared to power generators based on photovoltaics and thermoelectrics. Furthermore, a well-designed TEG can be used for harvesting low-grade thermal energy. Due to the above merits, TEGs, especially the traveling-wave ones, have great prospects in solar energy exploitation, waste heat recovery, and combined heat and power systems, etc.

The first traveling-wave TEG was built by Backhaus et al. [16] in 2004, which can supply an electric power of 58 W with a thermal-to-electric efficiency of 15%. The long standing-wave resonator in traditional traveling-wave thermoacoustic engines [10] was completely replaced by the linear alternators. The working principle, the tested powers and piston strokes were presented briefly. A small traveling-wave TEG, which was modified from a coaxial-type free-piston Stirling engine, was later developed by Sunpower, Inc. in 2008. However, only the power output of 50 W was mentioned and no further details were given. [17]. Since 2008, Luo et al. [18-21] have conducted a series of work on traveling-wave TEGs, and the obtained electric powers were

improved from about 100 W in 2008 to more than 1 kW recently. The experimental powers and efficiencies, and the acoustic impedance matching of the systems were presented and analyzed. Yu et al. [22, 23] were engaged in the development of low-cost TEGs that use loudspeaker as the acoustoelectric convertor. The details of the design, the effects of a tuning stub on the performances were given and analyzed. The obtained maximum electric power was 11.6 W when atmosphere air was used as the working gas. Recently, Kang et al. [24] built a two-stage traveling-wave TEG with two loudspeakers as alternators. One loudspeaker was placed inside the loop while the other one was installed through a branched stub. The distributions of acoustic fields in the system, and the effects of the stub length on the performances were conducted numerically and experimentally. An electric power of 204 W and a thermal-to-electric efficiency of 3.43% were achieved in the experiments. In 2013, Sun et al. [8] investigated the effects of the mechanical and electric resonances of the linear alternators on the performances of a traveling-wave TEG. A maximum electric power of 345.3 W and a highest thermal-to-electric efficiency of 12.33% were achieved under the resonance conditions. Though several prototypes of TEG have been built since 2004, comprehensive studies on the operating characteristics, especially the energy analysis of TEGs, are still lacking up to now, which limits the understanding of the underlying mechanisms and the further improvements of such systems. Besides, the improvements of the performance by replacing the large lossy resonator with linear alternators have not yet been fully conducted, especially for large TEGs up to more than hundreds watts.

In the present study, a traveling-wave TEG capable of generating about 500 W electric power is built and tested. The operating characteristics of the TEG are then studied under different working conditions both experimentally and numerically. The tested parameters, including piston displacement of alternator, pressure amplitudes, electric power, thermal-to-electric efficiency, et al., are presented in detail and compared with the numerical results. The variation trends of the output performances are further analyzed in the perspective of acoustic impedances. Particularly, distributions of various dissipations in the TEG are quantified and analyzed to give a clear evaluation of the losses. Further improvements of the TEG by replacing the resonator with linear alternators of large swept volume are finally conducted numerically.

2. Experimental setup

The experimental TEG is composed of a traveling-wave thermoacoustic engine and two LAs, as shown in Fig. 1. The thermoacoustic engine consists of a main ambient heat exchanger (MAHX), a regenerator (REG), a hot heat exchanger (HHX), a thermal buffer tube (TBT), a secondary ambient heat exchanger (2AHX), a feedback tube, and a resonator. The main geometric dimensions of the components are listed in Table 1. The MAHX is of shell-and-tube type with working gas flowing inside the thin stainless steel tubes. The total number and inner diameter of the tubes are 301 and 2 mm, respectively. Chilling water at about 12 °C flows over the thin tubes. The 2AHX is also of shell-and-tube type; the inner diameter of tubes is 3 mm; the total porosity is 0.179. The regenerator is filled with stainless steel screens with a porosity of 0.74 and a hydraulic radius of 49.8 μm. The HHX is of fin type with a porosity of 0.361 and the fin spacing is 1 mm. The core part, transferring heat to the working gas, of the HHX is made of copper. Dozens of heating resistors are inserted into the drilled holes of the HHX to provide the heating power. Two moving-magnet LAs, which are supplied by Lihan Thermoacoustic Technologies Co. Ltd, are installed symmetrically at the resonator near the tee. The parameters of the LAs #1 and #2 are listed in Table 2. The coils of the LAs are connected in series with a variable load resistance R_l and an electric capacitance C_e. The photographs of the thermoacoustic torus, one of the LAs, MAHX and HHX are given in Fig. 2.

When a temperature ratio across the REG exceeding the critical value is established, the working gas oscillates spontaneously with a constant frequency, and converts the input thermal energy into acoustic power. As shown by the arrows inside the thermoacoustic torus in Fig. 1, the acoustic power circulates clockwise, and is amplified due to the thermoacoustic conversion in the REG. A portion of the amplified acoustic power feeds back into the REG through the feedback tube, and the rest enters the LAs and the resonator to generate electric power and cause useless dissipations respectively.

In the experiments, a power meter with an accuracy of ±0.2% was used to measure the output electric power, the voltage of the load resistance, and the current in the circuit. The input heating power was measured by power meters with accuracies of ±0.5%. The

temperatures and the flow rate of the chilling water flowing in and out of the MAHX were measured by two calibrated K-type thermocouples and a turbine flowmeter with an accuracy of ±1%, respectively. The solid temperature of the HHX was also measured by a K-type thermocouple. The dynamic pressures of P1, P2 and P3 were measured by three PCB piezoelectric pressure sensors (model 102B15). The displacement amplitude x_1 of the LA #2 was deduced by the amplitude p_1 of P3 using the relationship of $x_1 = p_1 V_b / \gamma p_0 A$, where γ is the ratio of specific heats and p_0 is the mean pressure. The mean pressure of the system was measured by a piezoresistive pressure sensor supplied by

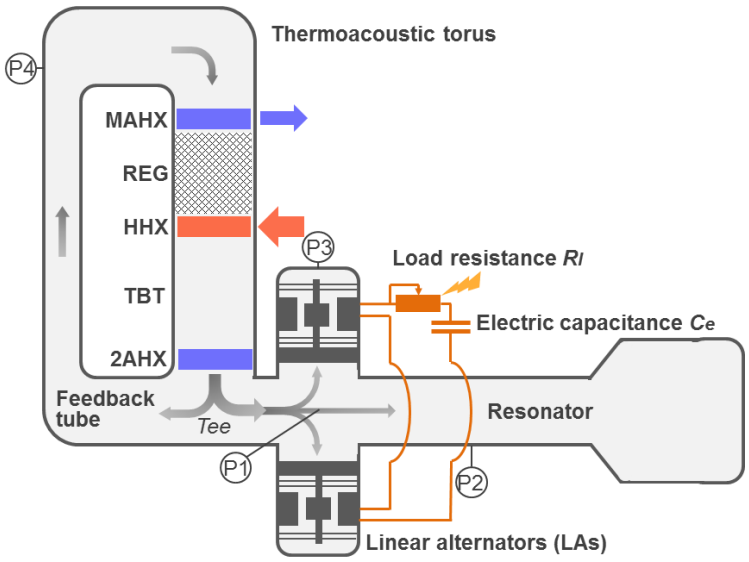

Fig. 1. Schematic of traveling-wave thermoacoustic electric generator.

Table 1. Main geometric dimensions of traveling-wave thermoacoustic engine.

Component		Diameter/m	Length/m
MAHX		0.09	0.056
REG		0.09	0.074
HHX		0.09	0.12
TBT		0.1	0.291
2AHX		0.1	0.02
Feedback tube	Tube near tee	0.09	0.295
	Cone	/	0.095
	Tube	0.076	0.28
	Cone	/	0.1
	Tube above MAHX	0.1	0.6767
Resonator	Tube near tee	0.09	0.095
	Cone	/	0.1
	Tube	0.1	2.3
	Cone	/	1.31
	Tube	0.261	0.52

Table 2. Parameters of linear alternators.

Parameters	Lihan #1	Lihan #2	modified Qdrive 2s241PWG*
Force factor Bl (N/A)	90	90	54
Winding inductance L_e (mH)	268	263.4	26
Winding resistance r_e (Ω)	3.58	3.56	1
Mechanical stiffness K (N/m)	189235	188844	175000
Mechanical resistance R_m (Ns/m)	5	2	35
Moving mass M (kg)	1.097	1.079	5.6
Piston area A (cm^2)	19.635	19.635	387.16
Back volume V_b (L)	1.63	1.63	78.5

*This is a pair of the same LAs in an opposite arrangement. The parameters here are for one LA. The original moving mass, piston area, and back volume are 4.2 kg, 91.61 cm^2, and 55 L, respectively.

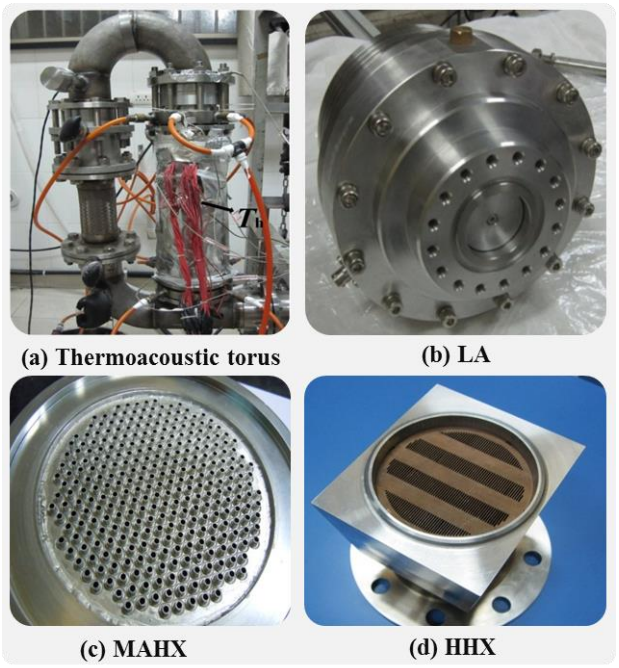

Fig. 2. Photographs of key components of the traveling-wave thermoacoustic electric generator: (a) thermoacoustic torus; (b) LA; (c) MAHX; (d) HHX.

Huba Control (model 511.933003142) with an accuracy of ±0.3%, as shown by P4. The output electric power and other parameters were measured when the system worked steadily at constant heating temperatures.

3. Results and discussions

As illustrated in our previous work [8], the resonance characteristics of the TEG are critical to the performance of the system. Thus, two measures are taken here to make the TEG work at resonance states. Firstly, helium gas is used as the working medium. As a

result, the operating frequency is about 65 Hz, which is close to the mechanical resonance frequencies of the LAs. A near mechanical resonance state is then achieved. Secondly, an electric capacitance of 9.6 μF is connected in the circuit to offset the large winding inductances of the LAs, and the electric resonance state is also achieved when the TEG works at about 65 Hz. Except for the experimental analysis, a numerical model is also built based on DeltaEC (Design Environment for Low-amplitude ThermoAcoustic Energy Conversion) [10, 23, 25-28].

3.1. Pressure, displacement and current amplitudes

Fig. 3 shows the pressure amplitudes of P1 and P2, the locations of which are denoted in Fig. 1 respectively. The acoustic field in resonator is close to a quarter-wavelength standing-wave one, with P1 near the pressure antinode and P2 near the pressure node. Thus, the pressure amplitude of P1 is much larger than that of P2, as shown in Fig. 3. Both of the pressure amplitudes increase largely when the load resistance is decreased. The calculated results agree well with the experimental ones in both tendencies and magnitudes. The output electric power of the LAs is approximately proportional to the load resistance and the square of the pressure amplitude in front of the LAs when both the mechanical and electrical resonances are achieved, according to its expression [8]. Thus, when reducing the load resistance, the output electric power first increases due to the rapid increase of the square of the pressure amplitude, and then decreases as a result of the small load resistance. It should be noted that the acoustic power dissipations in the TEG are also proportional to the square of the pressure

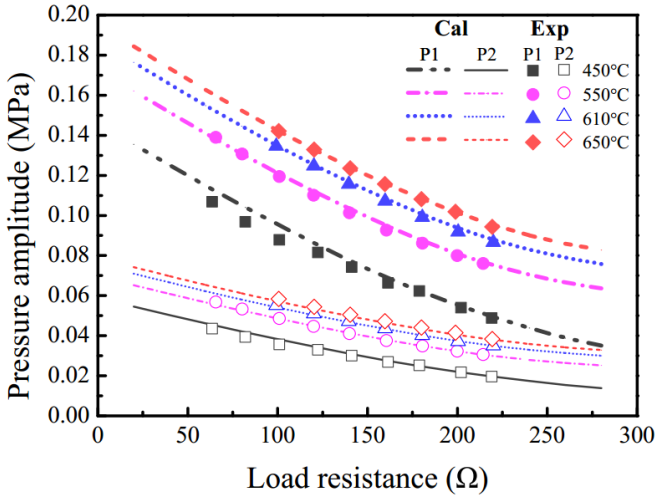

Fig. 3. Pressure amplitudes of P1 and P2 vs load resistance at different heating temperatures when mean pressure is 2.48 MPa.

amplitudes. Therefore, small load resistances have a negative effect on the thermal-to-electric efficiency due to the much larger dissipations.

The piston displacement amplitude of LA #2 and the current amplitude are shown in Fig. 4 and Fig. 5, respectively. As shown in Fig. 4, the displacement amplitude increases with the load resistance in the ranges of 20~280 Ω when the heating temperature is higher than 450 °C. When the heating temperature is 450 °C, the displacement amplitude first increases and then decreases with the load resistance. The displacement amplitudes at these temperatures are all within the displacement limit of the LAs, which is 6.5 mm. As shown in Fig. 5, the dependence of current on the load resistance is completely different from that of the displacement. It decreases with the load resistance at all the heating temperatures. Thus, the load resistance should not be

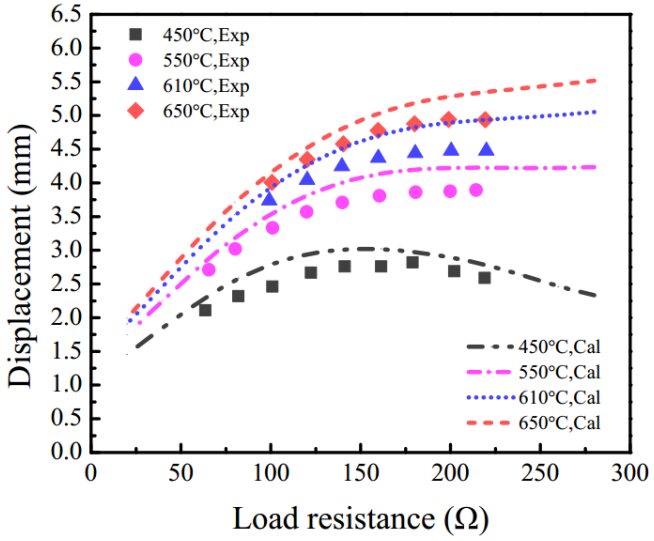

Fig. 4. Piston displacement of LA #2 vs load resistance at different heating temperatures when mean pressure is 2.48 MPa.

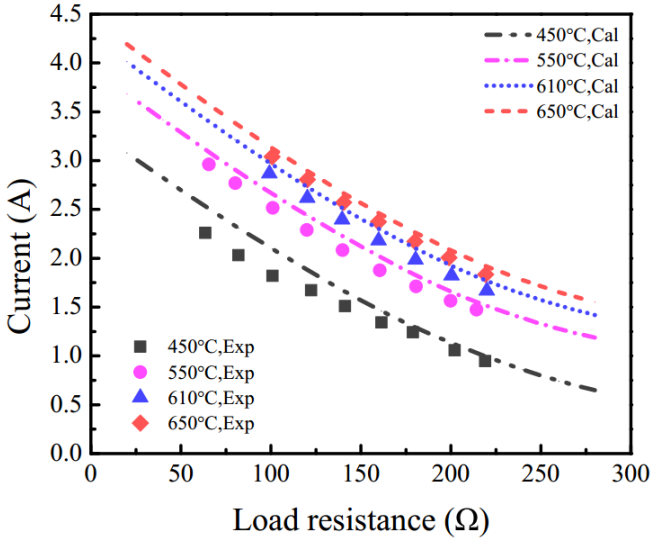

Fig. 5. Current vs load resistance at different heating temperatures when mean pressure is 2.48 MPa.

too small in case the current exceeds the upper limit of 4 A. The good agreements between the calculations and the experiments in the displacements and the currents further indicate that the working characteristics of the TEG are well presented by the numerical model.

3.2. Electric power

Fig. 6 shows the electric power generation of the TEG with respect to the load resistance at different heating temperatures when the mean pressure is 2.48 MPa. As shown, the calculated results agree well with the experimental ones at all the heating temperatures. The deviations are typically less than 13%. The electric power first increases, and then decreases with the load resistance due to the combined effects of

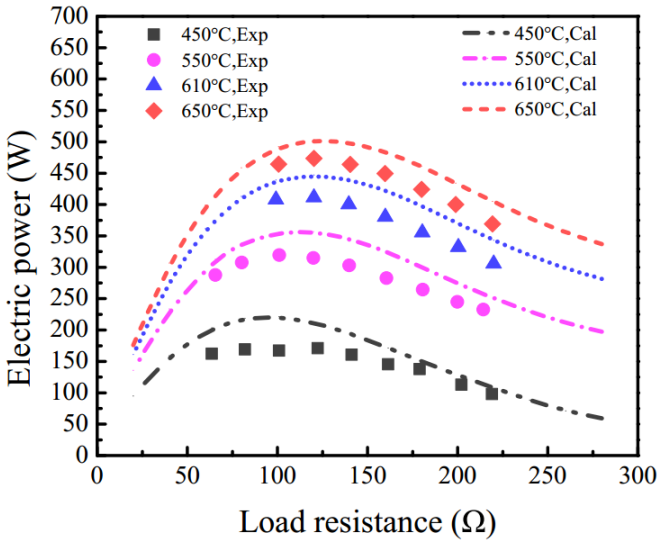

Fig. 6. Electric power vs load resistance at different heating temperatures when mean pressure is 2.48 MPa.

pressure amplitude and load resistance, as analyzed above in Fig. 3. The optimal load resistances are in the range from 100 Ω to 120 Ω, and rise slightly with the heating temperature due to the tiny increase of the operating frequency. When the heating temperature is fixed at 650 °C, the maximum electric power of the TEG at this mean pressure is 473.6 W with a load resistance of 120 Ω.

The variation trends of the electric power can be essentially explained from the perspective of acoustic impedance. All thermoacoustic systems can be analogized into AC circuits due to their similar oscillation features of the parameters, such as pressure and voltage, etc [5]. For the TEG, the regenerator acts as a power source, while the LAs

act as a load acoustic impedance which has a real part and an imaginary one. Fig. 7 shows the calculated acoustic impedance of the LAs at different load resistance. When the load resistance is decreased from 220 Ω to 100 Ω, the imaginary acoustic impedance of the LAs changes from −2.8 MPa·s/m^3 to 1.55 MPa·s/m^3. The output acoustic powers of the thermoacoustic engine at different real acoustic impedances are given in Fig. 8 when the imaginary acoustic impedance is fixed at −3 MPa·s/m^3, 0 MPa·s/m^3, and 1.5 MPa·s/m^3, which covers the impedance range of the LAs stated above. It shows that the variation trends and the magnitudes of the output acoustic powers with respect to the real acoustic impedance are approximately the same at these imaginary acoustic impedances. Thus the real acoustic impedance dominates the variation trend of the output acoustic power at these conditions. When the load resistance decreases from 220 Ω to 100 Ω, the real acoustic impedance of the LAs increases from 9.6 MPa·s/m^3 to 18.6 MPa·s/m^3, as shown by the solid line in Fig. 7. According to the curves in Fig. 8, the corresponding output acoustic power of the thermoacoustic engine first increases and then decreases slightly after reaching the maximum value at the above acoustic impedance range. Fig. 9 shows the dependences of the electric power and the thermal-to-electric efficiency of the integrated TEG on the load acoustic impedance. The generated electric power has similar tendency as the acoustic power when the acoustic impedance of the LAs increases. The above analysis shows that the relationships between the powers and load acoustic impedance eventually shape the tendency of the electric power curve in Fig. 6. In all, adjusting the load resistance

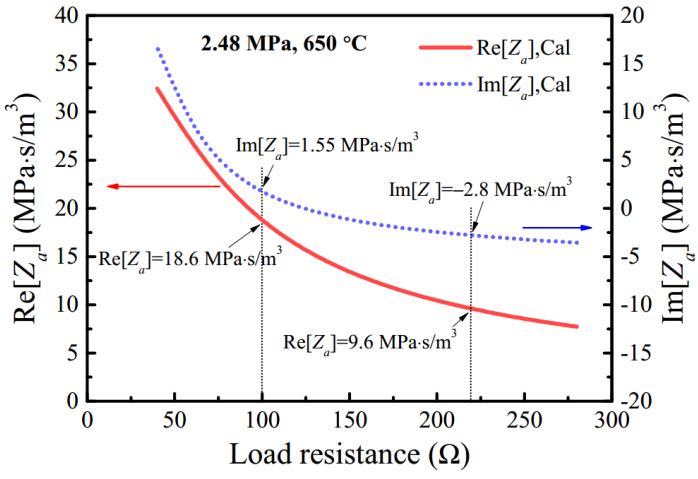

Fig. 7. Acoustic impedance of LAs #1 and #2 at different load resistance when mean pressure is 2.48 MPa.

essentially changes the acoustic impedances of the LAs, which then determines the output capability of the engine, and further affects the generated electric power.

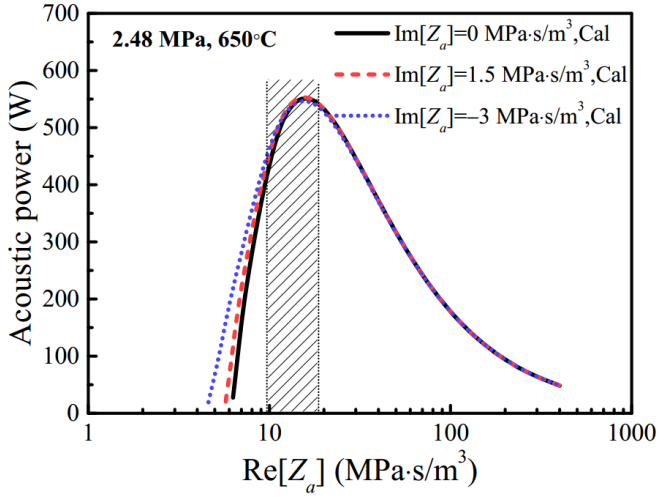

Fig. 8. Output acoustic power of traveling-wave thermoacoustic engine vs load acoustic impedance at the connecting position of LAs.

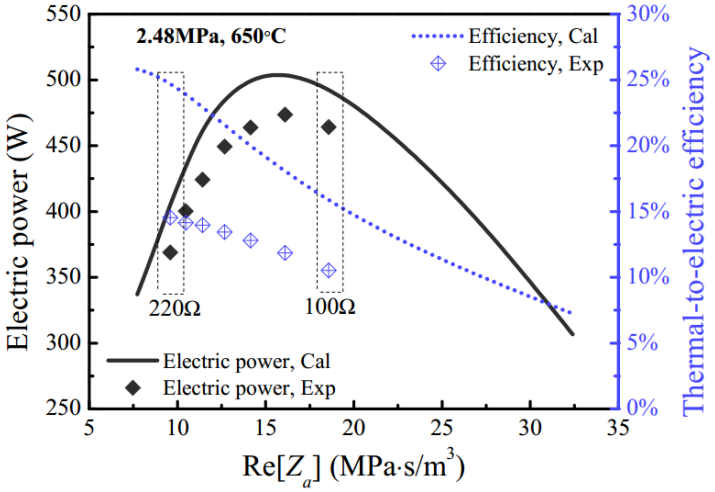

Fig. 9. Electric power and thermal-to-electric efficiency of traveling-wave thermoacoustic electric generator vs load acoustic impedance at the connecting position of LAs.

3.3. Heating and heat release powers

The heating powers of the HHX and the heat release powers of the MAHX are shown in Fig. 10. The red and blue bars are the calculated results, and the connected points are the experimental ones. The tendencies of the experimental and calculated results agree well with each other. When decreasing the load resistance, the heating power and the heat release power both increase. This is because that the pressure amplitudes at lower load resistances are much larger, as illustrated in Fig. 3, and the heat transfer rates in the heat exchangers increase remarkably compared to that at larger load resistances. It is noted that the heating and heat release powers in the experiments are all

larger than that of the calculations. The deviations mainly result from the underestimated heat losses from the HHX in the modeling, including the heat radiation and convection to the air and the 2AHX through the TBT, and the heat conduction through the pipes and the REG. Moreover, we use backup heating elements to increase

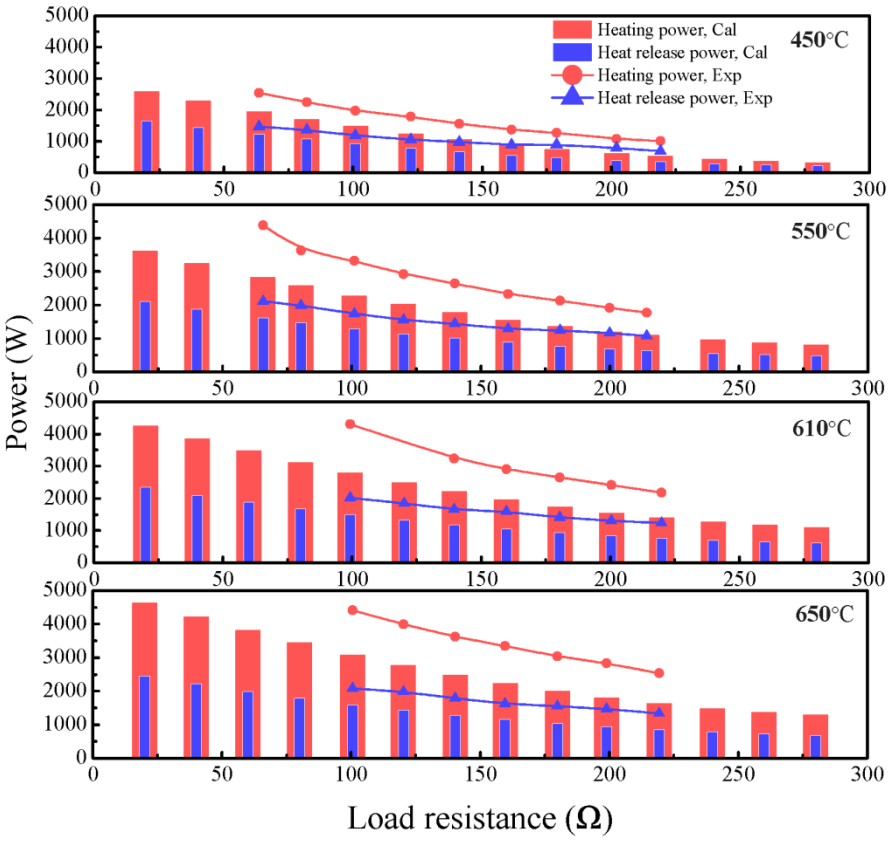

Fig. 10. Heating power and heat release power vs load resistance at different heating temperatures when mean pressure is 2.48 MPa.

the heating power, which are installed in the periphery of the HHX. These backup heating elements have a much worse heating performance because of the longer heat conduction route.

3.4. Energy losses

According to the energy conservation principle, a part of the heating power is converted into the acoustic power in the REG, while the rest is taken away by the chilling water or dissipated by the heat losses. Some of the net generated acoustic power is converted into electric power by the LAs, and the rest is dissipated in the tubes, the heat exchangers and the LAs by various mechanisms, including the viscous effects, thermal-relaxation effects, Joule heat loss of the circuit, etc. Fig. 11 shows the

calculated dissipation distributions of the generated acoustic power when the heating temperature is 650 °C at 2.48 MPa. The experimental electric powers are also given for comparison, as indicated by the triangular symbols. As shown, the ratio of the electric power to the net generated acoustic power, i.e. the sum of all the dissipation losses and the electric power in Fig. 11, is relatively small at low load resistances, and becomes larger with the load resistance. This indicates that a large amount of the generated acoustic power is not converted into electric power but dissipated at small load resistances, which is because of the large pressure amplitudes as shown by the loss bars here and illustrated in Fig. 3. Therefore, it is effective to intensify the pressure oscillation and increase the acoustic power generation by decreasing the load resistance. However, only a small portion of the generated acoustic power is eventually converted into electric power under these conditions, which on the contrary limits the thermal-to-electric efficiency.

As shown in Fig. 11, the resonator is the largest source of acoustic power dissipations, and is responsible for more than half of the total losses in the TEG. The losses in the resonator mainly include the viscous dissipations, thermal relaxation losses, minor losses and nonlinear losses, etc., and become more severe at large pressure amplitudes. When the TEG works at low load resistances, the pressure amplitudes are so large that a huge amount of acoustic power losses occur in the resonator. For example, when the load resistance is 20 Ω, the acoustic power loss in the resonator is up to 1253 W, which takes up to 53% of the generated acoustic power according to the calculations. However, the generated electric power in the calculation at this working condition is only 176 W. When the load resistance is increased to 120 Ω, the acoustic power loss in the resonator decreases to 480 W, while the electric power reaches up to 503 W. It is indicated that the acoustic power losses and electric power generation can be effectively adjusted by varying the load resistance.

According to the calculations, the losses in the feedback tube and the TBT are also very remarkable due to the large surface areas in these tubes. It’s worth noting that the acoustic power loss in the HHX is even larger than that in the TBT. When the load resistance is adjusted from 20 Ω to 280 Ω, the loss in the HHX takes up to about 7%~9% of the total generated acoustic power. The main reason is that the oscillating velocity

through the HHX is very large due to the small open area and the high temperature. The peak velocity is up to 10~20 m/s, which is more than double that of the TBT. Besides, the length of the HHX is designed relatively long to supply sufficient heating power, which causes additional loss. From this perspective, the geometric dimensions of the HHX need to be optimized to decrease the acoustic power loss and enhance the heat transfer performance. The acoustic power losses in the AHXs are much smaller due to the much shorter lengths and lower velocities. The losses from the LAs mainly result from the mechanical frictions of the pistons and the Joule heating in the coils. The mechanical loss of the LAs increases with the load resistance, due to the increase of the piston displacements and oscillating velocities, as shown in Fig. 4. On the contrary, the Joule heat loss of the LAs becomes larger when reducing the load resistance, due to the variation trend of the current as shown in Fig. 5.

In all, the acoustic power dissipation in the resonator is dominant in the TEG, and has a serious negative effect on the thermal-to-electric efficiency. Effective measures should be explored to decrease the huge acoustic power loss in the long resonator. Possible approaches include optimizing the shape of the resonator, smoothing the internal surface of the resonator, and even replacing the resonator with LAs having enough swept volume or with pistons driving crank-rod mechanisms.

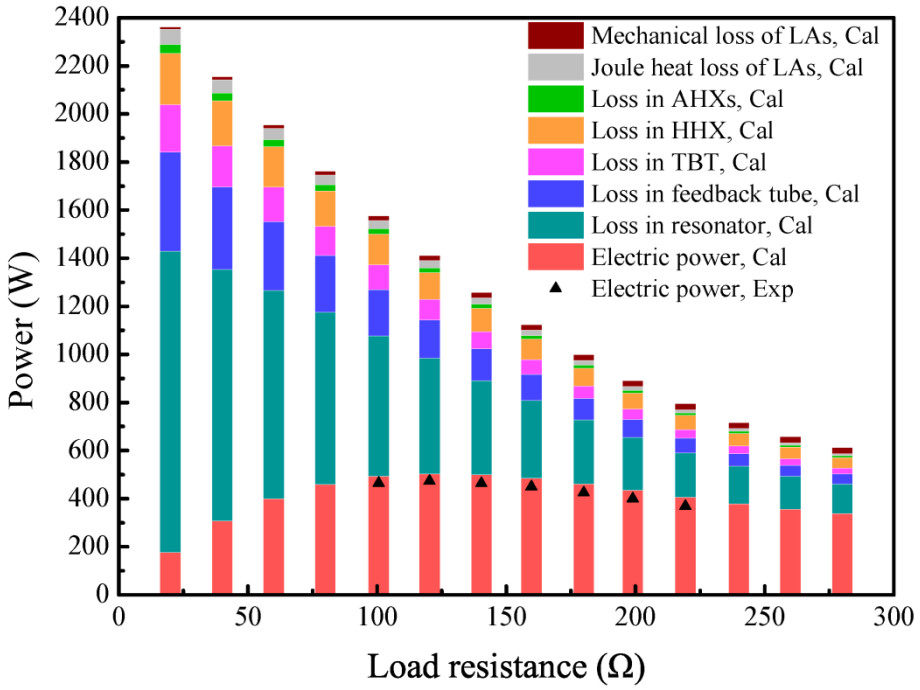

Fig. 11. Dissipation distributions vs load resistance when the heating temperature is 650 °C at 2.48 MPa.

3.5. Thermal-to-electric efficiency

The variation trends of the thermal-to-electric efficiency with the load resistance are shown in Fig. 12. As shown, the tendencies of the calculated efficiencies agree with the experimental results within the whole range of interest. For example, when the heating temperature is 450 °C, the calculated efficiency increases with load resistance below 200 Ω, and then has a rapid decrease when load resistance exceeds 200 Ω. The experimental result has the same tendency. It is also found that the optimal resistance to reach the highest efficiency gets higher with the heating temperature. When the heating temperature is higher than 450 °C, the optimal load resistances for the thermal-to-electric efficiency increase to more than 280 Ω. Compared with Fig. 6, the optimal load resistances needed for the efficiency are much larger than that for the electric power. This is because the optimal real acoustic impedance for thermal-to-acoustic efficiency is smaller than that for output power, as shown in Fig. 13, which means the required load resistance is much larger. Besides, the acoustic-to-electric efficiency of the LAs stays stably at around 90%. As a result, when increasing the load resistance from 100 Ω to 220 Ω, the thermal-to-acoustic efficiency as well as the overall thermal-to-electric efficiency both increase as the corresponding real acoustic impedance decreases, as denoted by the shadow area in Fig. 13 and Fig. 9. In the experiments, the acoustic impedance can not reach the optimal value, as shown in Fig. 9, due to the limited adjustable range of the load resistance for ensuring the displacements and the currents in the safety ranges. So the efficiency fails to reach its maximum value in the experiment when the heating temperature is 650 °C, as shown in Fig. 12. Therefore, the directions for designing, optimizing the TEG can be clearly shown by the acoustic impedance analysis method.

The thermal-to-electric efficiencies at low load resistances are very limited due to the huge viscous dissipations caused by the large pressure amplitude inside the system, as discussed before. It is apparently shown that there still exists a large efficiency discrepancy between calculations and experiments. In experiments, the obtained highest thermal-to-electric efficiency at 2.48 MPa is 14.5% when the heating temperature is 650 °C, but the corresponding calculated result under this working condition is 24.7%.

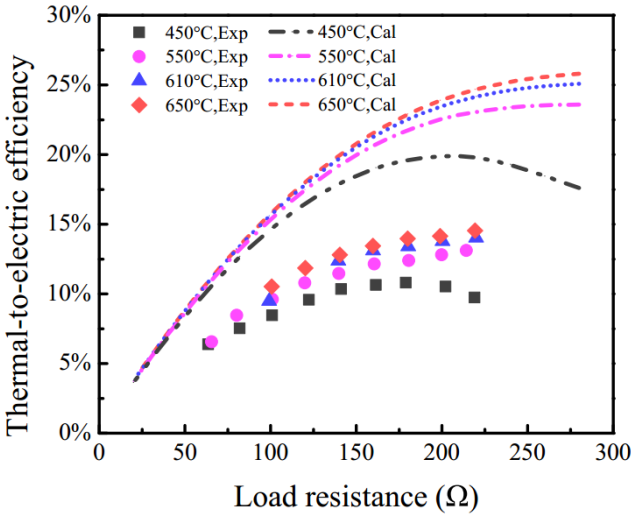

Fig. 12. Thermal-to-electric efficiency vs load resistance at different heating temperatures when mean pressure is 2.48 MPa.

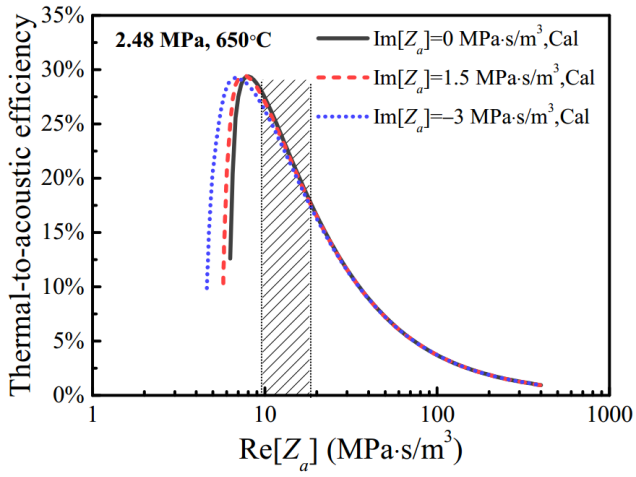

Fig. 13. Thermal-to-acoustic efficiency of traveling-wave thermoacoustic engine vs load acoustic impedance at the connecting position of LAs.

The deviations mainly result from the underestimated heat losses and the limited heating performance of the HHX, as analyzed above in Fig. 10. Besides, the losses caused by the membrane above the MAHX have not been included yet in the calculation.

3.6. Effects of mean pressure and heating temperature

As analyzed above, the generated electric power can be increased significantly by increasing the driving pressure amplitude of the LAs for a given load resistance. Thus, increasing the heating temperature and the mean pressure to enhance the pressure oscillations are both beneficial for the electric power generation. In the experiments, the

heating temperature is limited within 650 °C for safety reasons. Fig. 14 shows the relationships between the maximum electric power, the highest thermal-to-electric efficiency, and the heating temperature when the mean pressure is 2.48 MPa and 3.20 MPa, respectively. The electric powers and the efficiencies are both approximately in linear relationships with the heating temperature but with different slopes. The electric power is much more strongly affected by the heating temperature. For example, the electric power is only 170.9 W when the heating temperature is 450 °C with the mean pressure of 2.48 MPa in the experiments, while it reaches 473.6 W when increasing the heating temperature to 650 °C. The slope of the electric power at 2.48 MPa is 1.51 W/K in the experiments, and that in the calculation is 1.41 W/K. The thermal-to-electric efficiency increases from 10.8% to 14.5% when the heating temperature is increased from 450 °C to 650 °C in the experiments. The calculation shows that the electric power can be increased significantly when the mean pressure is increased from 2.48 MPa to 3.20 MPa to increase the output capacity of the engine, as the driving pressure amplitude and the power density both increase. When the mean pressure is 3.20 MPa, the electric power at 650 °C reaches up to 776.5 W, with an increase of 54.2% compared to that of 2.48 MPa, according to the calculations. The calculated slope is increased to 2.16 W/K, showing an increase of 53.2%. Efficiency is also improved to some extent, but not as much as that of the electric power. Hence, increasing the mean pressure so as to increase the power density is an effective way of improving the performances of the TEG.

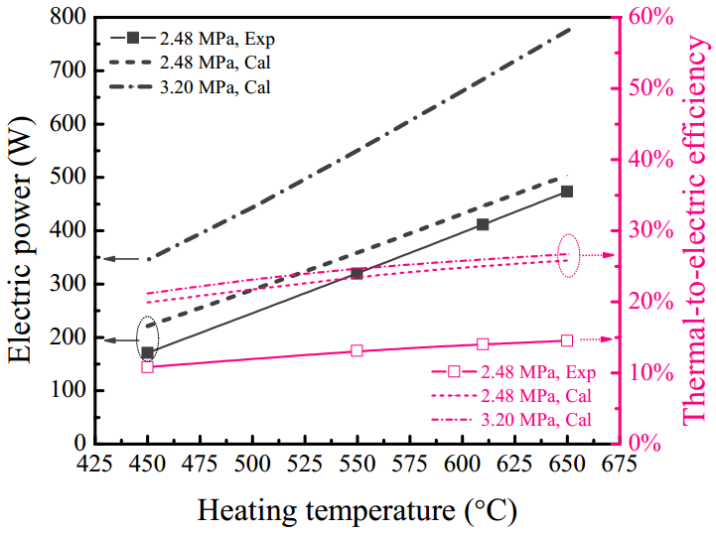

Fig. 14. Electric power and thermal-to-electric efficiency vs heating temperature at mean pressures of 2.48 MPa and 3.16 MPa.

3.7. Further improvements through torus-LAs direct-coupling design

As analyzed above, the long gas resonator in traditional traveling-wave thermoacoustic engines brings about huge acoustic losses and makes the system less compact. One of the effective approaches to improve the system is to replace the resonator with mass-spring components with a sufficiently large swept volume, such as LAs. The configuration is similar to that in Fig. 1, but without the resonator. In the following section, a pair of LAs with appropriate acoustic characteristics is designed to directly couple with the aforementioned thermoacoustic torus to investigate the potentials of performance improvements through this approach.

In the traveling-wave thermoacoustic engine, the torus is essentially an acoustic compliance and transfers energy between the inertance part periodically, i.e. the gas resonator in traditional system, or the LAs in the torus-LAs direct-coupling design. The working frequency is mainly determined by magnitudes of the compliance and inertance. For the traveling-wave TEG shown in Fig. 1, the inertance impedance coupled to the torus, which is the combination of the acoustic impedances of the LAs and the gas resonator, stays almost constant at 0.572 MPa·s/m^3 whatever the load resistances are when it is at 2.48 MPa and 650 °C according to the calculations. This is because the inertance part of the gas resonator is only about one-tenth of the inertance of the LAs, and thus more dominant when they are coupled in parallel. As a result, the frequency also stays stably around 66 Hz. For the convenience of the comparisons, the working conditions in the design are set the same as that of the old system: the mean pressure, heating temperature and working frequency are fixed at 2.48 MPa, 650 °C and around 66 Hz, respectively. This means that the inertance impedance of the LAs in the new design should be 0.572 MPa·s/m^3 to maintain this frequency.

The requirements for the real acoustic impedance to directly couple with the thermoacoustic torus are then calculated, as shown in Fig. 15. The imaginary acoustic impedance is fixed at 0.572 MPa·s/m^3, and the operating frequency is thus around 66 Hz, which is shown in Fig. 16. As shown in Fig. 15, the required real acoustic impedance to get an optimal output acoustic power from the torus is about 0.0167 MPa·s/m^3, while that for the efficiency is much larger, i.e. around 0.0361 MPa·s/m^3. To

reach a balance between acoustic power and efficiency, the reasonable real acoustic impedance of the LAs is within the two optimal values.

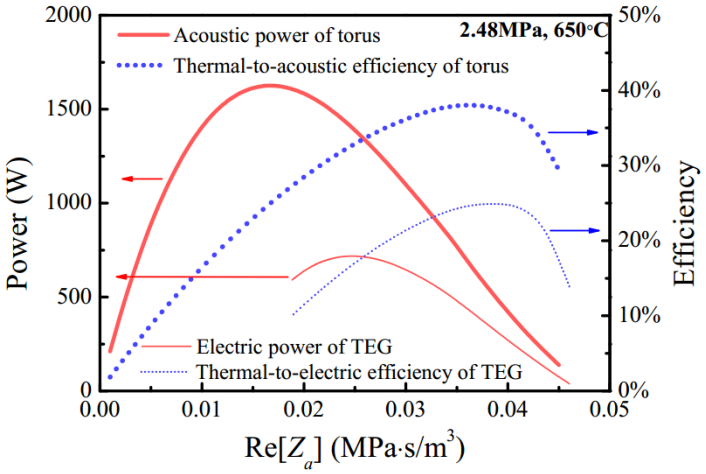

Fig. 15. Dependences of output performances of thermoacoustic torus and the torus-LAs direct-coupling thermoacoustic electric generator on real acoustic impedance of acoustic load.

Aside from the above requirements of the frequency and the acoustic impedances, the volume flow rate is another important parameter that determines whether the acoustic load can match the torus. For example, low-voltage electronic devices can never be used in high-voltage circuits even if the electrical impedances are appropriate for the circuits. Therefore, the requirements for the volume flow rate of the thermoacoustic torus are calculated and shown in Fig. 16. The required volume flow rates are 0.44 m^3/s and 0.19 m^3/s respectively when the maximum acoustic power and thermal-to-acoustic efficiency are achieved, as shown by the points A and B. The large volume flow rate mainly results from the low power transfer capability of the standing-wave acoustic field at the output port of the torus as shown by blue dotted line in Fig. 16.

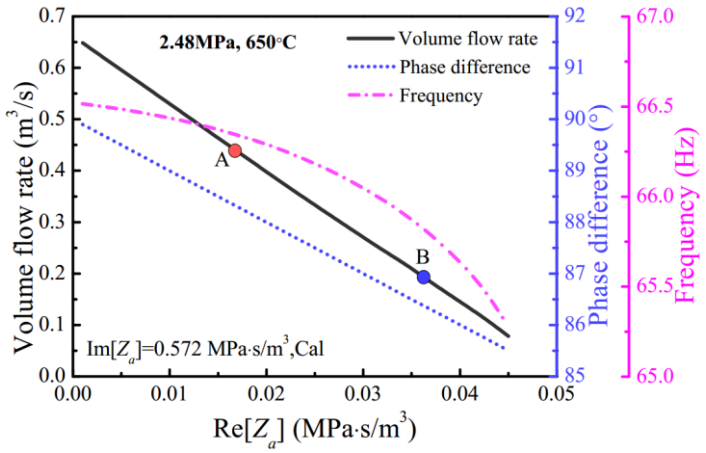

Fig. 16. Dependances of output volume flow rate, phase difference and operating frequency on real acoustic impedance of acoustic load.

Compared with the real acoustic impedance of the LAs #1 and #2 shown in Fig. 7, the required one for the torus-LAs direct-coupling design is smaller by three orders of magnitude. Besides, the maximum volume flow rate supplied by the LAs #1 and #2 is only 0.01 m^3/s, which is far less than the required one of the torus, as analyzed above. Therefore, the piston diameters and displacements of the new LAs should be much larger. A pair of commercial LAs (Qdrive 2s241PWG) is chosen to meet the requirement of volume flow rate [29]. In order to adjust the acoustic impedance to the desired range, the moving mass, piston area, and back volume of the LAs have been modified correspondingly, which are practically feasible. The parameters of the modified LAs are listed in Table 2 too. The calculated acoustic impedances of the modified LAs at about 66 Hz are shown in Fig. 17. As shown, the imaginary acoustic impedance is close to 0.572 $MPa \cdot s/m^3$, and the real one can be adjusted to be within the required range. It indicates that the modified acoustic impedance is appropriate for coupling with the torus.

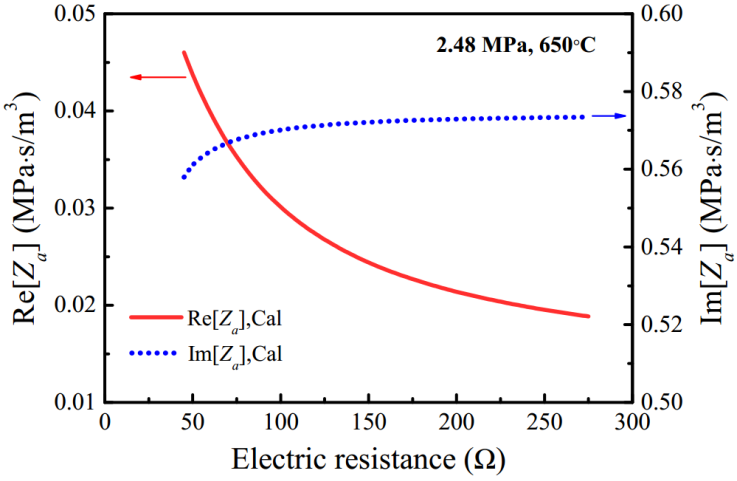

Fig. 17. Acoustic impedance of the modified Qdrive 2s241PWG at different load resistance when mean pressure is 2.48 MPa.

By adjusting the outlet impedance of the thermoacoustic torus and the inlet impedance of the LAs to be the same, the two sub-units can then be coupled in the model. As analyzed above, the volume flow rate should be checked to ensure whether the LAs meet the requirements. Fig. 18 shows the pressure amplitude, displacement, and volume flow rate of the torus-LAs direct-coupling TEG. The displacement and the volume flow rate are equivalent and can be converted to each other. As shown, the volume flow rate is within 0.41 m^3/s at the range of interest. The corresponding

displacements of the LAs are within 13 mm, which are reasonable values and indicate that the volume flow rates of the sub-units match each other. Therefore, the modified LAs are appropriate for coupling with the torus from all the three key aspects of matching: frequency, acoustic impedance, and volume flow rate.

Fig. 19 and Fig. 20 show the electric power and thermal-to-electric efficiency of the torus-LAs direct-coupling TEG at different load resistances, respectively. The dependance of the electric power and the efficiency of the system on the corresponding acoutic impedance are given in Fig. 15. As shown in Fig. 19, the calculated maximum output electric power reaches 718 W at 150 Ω when the mean pressure is 2.48 MPa, corresponding to an increase of 42.6% compared with the old design. However, as the LAs are not originally designed for this application, the acoustic-to-electric efficiency after the modifications is very limited, especially at high load resistances, as shown in Fig. 20. For example, when the system works at its most powerful output point, the corresponding acoustic-to-electric efficiency is only 50.7%. Besides, as the conversion efficiency of the LAs is even lower at larger load resistances, i.e. lower real acoustic impedance as shown in Fig. 15, a larger amount of the output acoustic power of the torus is not converted into electric power but dissipated by the LAs. As shown in Fig. 20, the highest thermal-to-electric efficiency is about 25%, which is comparable with the results of the old design even though the acoustic-to-electric efficiency of the LAs is very limited. Except from the low conversion efficiency of the LAs, another reason for the low thermal-to-electric efficiency at larger load resistances is the larger pressure amplitudes inside the system, which means that the dissipations in the torus also become larger, as shown in Fig. 18.

The performances of the system at a mean pressure of 3.20 MPa are also predicted, though the LAs are initially designed to couple with the torus at 2.48 MPa. The frequency increases from about 66.2 Hz to about 72.5 Hz, due to the decrease of the torus compliance with the mean pressure. The maximum electric power reaches 1005 W, while the result of the old design is only 776.5 W. The maximum thermal-to-electric efficiency at 3.20 MPa is similar to that at 2.48 MPa. The required load resistance for the same efficiency at 3.20 MPa is a littler smaller. A large space is still left for improving the output electric power and efficiency if more efficient LAs are specifically

designed to couple with the thermoacoustic torus. For example, if the efficiencies of the LAs are increased to 85% at the most powerful and the most efficient points of the system, the electric power and the overall efficiency can be increases up to 1204 W and 31.2% at 2.48 MPa respectively.

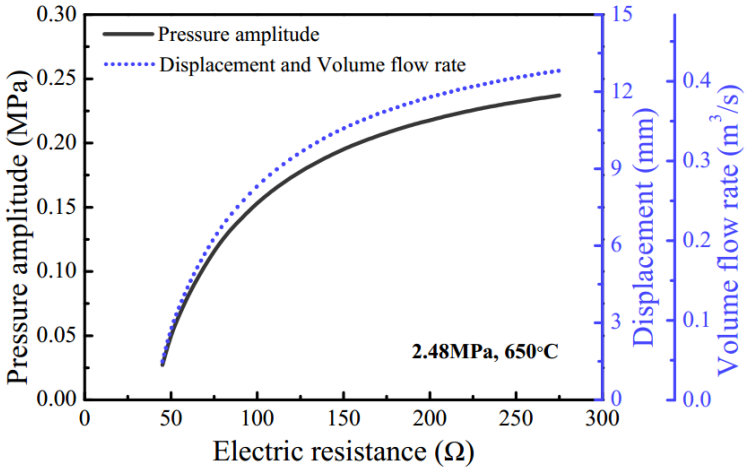

Fig. 18. Pressure amplitude, displacement, and volume flow rate of the torus-LAs direct-coupling thermoacoustic electric generator.

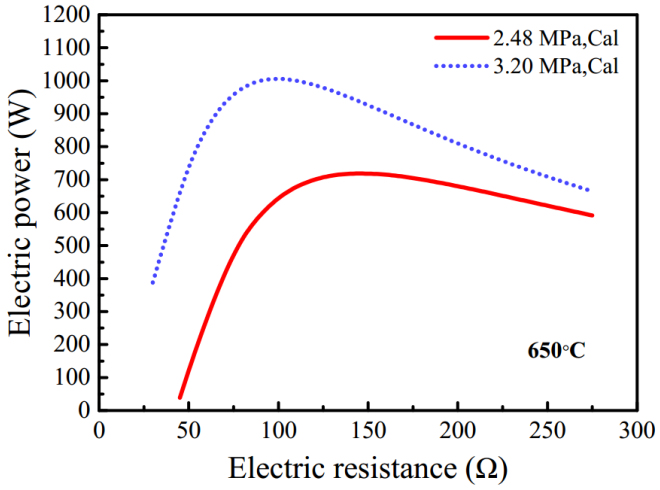

Fig. 19. Electric power of the torus-LAs direct-coupling thermoacoustic electric generator.

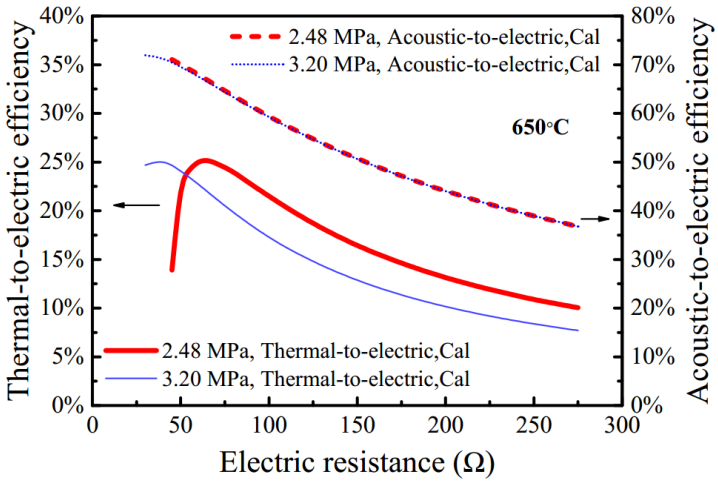

Fig. 20. Thermal-to-electric efficiency of the torus-LAs direct-coupling thermoacoustic electric generator.

4. Conclusions

A traveling-wave thermoacoustic electric generator capable of generating about 500 W electric power are numerically and experimentally studied. The performances of the system are predicted and tested at different working conditions. The important parameters, including pressure amplitude, displacement, electric power, thermal-to-electric efficiency, etc., are presented in detail and analyzed systematically. The optimal load resistances for the electric power are around 100 Ω~120 Ω, while those for the thermal-to-electric efficiency are much larger. The in-depth analysis from the perspective of acoustic impedances shows that the difference results from the different requirements for the acoustic impedances of the linear alternator to obtain the optimal power and efficiency. The distributions of power dissipations of the system are firstly illustrated quantitatively. It is shown that the acoustic power dissipations in the resonator are the dominant losses, especially at low load resistances. The acoustic power dissipations in the hot heat exchangers, thermal buffer tube, and the feedback tube are also very significant. As predicted, the acoustic power generation can be effectively improved by increasing the heating temperature and the mean pressure. Till now, the maximum electric power and the highest thermal-to-electric efficiency achieved experimentally at 2.48 MPa are 473.6 W and 14.5%, respectively. To further improve the performances, a pair of large commercial linear alternators are modified to couple with the thermoacoustic torus directly in numerical study. The calculated results indicate that the performance can be greatly improved after replacing the gas resonator with linear alternators, showing the great potential of the torus-LAs direct-coupling thermoacoustic electric generators.

Acknowledgments

This research is supported by National Natural Science Foundation of China under contract No. 51476136 and Zhejiang Provincial Natural Science Foundation of China under Grant No. Z1110222.

References

[1] Wang Y, Chen KS, Mishler J, Cho SC, Adroher XC. A review of polymer electrolyte membrane fuel cells: Technology, applications, and needs on fundamental research. Applied Energy. 2011;88:981-1007.

[2] Mercaldo LV, Addonizio ML, Della Noce M, Veneri PD, Scognamiglio A, Privato C. Thin film silicon photovoltaics: Architectural perspectives and technological issues. Applied Energy. 2009;86:1836-44.

[3] Backhaus S, Swift GW. A thermoacoustic Stirling heat engine. Nature. 1999;399:335-8.

[4] Gou X, Xiao H, Yang S. Modeling, experimental study and optimization on low-temperature waste heat thermoelectric generator system. Applied Energy. 2010;87:3131-6.

[5] Saadon S, Sidek O. A review of vibration-based MEMS piezoelectric energy harvesters. Energy Conversion and Management. 2011;52:500-4.

[6] Hsu CJ, Sandoval SM, Wetzlar KP, Carman GP. Thermomagnetic conversion efficiencies for ferromagnetic materials. Journal of Applied Physics. 2011;110:123923.

[7] Sun DM, Qiu LM, Zhang W, Yan WL, Chen GB. Investigation on traveling wave thermoacoustic heat engine with high pressure amplitude. Energy Conversion and Management. 2005;46:281-91.

[8] Sun DM, Wang K, Zhang XJ, Guo YN, Xu Y, Qiu LM. A traveling-wave thermoacoustic electric generator with a variable electric R-C load. Applied Energy. 2013;106:377-82.

[9] Luo EC, Ling H, Dai W, Zhnag Y. A high pressure-ratio, energy-focused thermoacoustic heat engine with a tapered resonator. Chinese Science Bulletin. 2005;50:284-6.

[10] Backhaus S, Swift GW. A thermoacoustic-Stirling heat engine: Detailed study. The Journal of the Acoustical Society of America. 2000;107:3148-66.

[11] Biwa T, Hasegawa D, Yazaki T. Low temperature differential thermoacoustic Stirling engine. Applied Physics Letters. 2010;97:-.

[12] Hu ZJ, Li ZY, Li Q, Li Q. Evaluation of thermal efficiency and energy conversion

567 of thermoacoustic Stirling engines. Energy Conversion and Management.
568 2010;51:802-12.
569 [13] Tijani MEH, Spoelstra S. A high performance thermoacoustic engine. Journal of
570 Applied Physics. 2011;110:093519.
571 [14] Shen C, He YL, Li YG, Ke HB, Zhang DW, Liu YW. Performance of solar
572 powered thermoacoustic engine at different tilted angles. Appl Therm Eng.
573 2009;29:2745-56.
574 [15] de Waele ATAM. Basic treatment of onset conditions and transient effects in
575 thermoacoustic Stirling engines. Journal of Sound and Vibration. 2009;325:974-88.
576 [16] Backhaus S, Tward E, Petach M. Traveling-wave thermoacoustic electric generator.
577 Applied Physics Letters 2004;85:1085-7.
578 [17] Oriti SM, Schifer NA. Recent Stirling Conversion Technology Developments and
579 Operational Measurements at NASA Glenn Research Center. 7th International Energy
580 Conversion and Engineering Conference (IECEC 2009). Denver, CO, USA2009.
581 [18] Luo EC, Wu ZH, Dai W, Li SF, Zhou Y. A 100 W-class traveling-wave
582 thermoacoustic electricity generator. Chinese Science Bulletin. 2008;53:1453-6.
583 [19] Wu ZH, Man M, Luo EC, Dai W, Zhou Y. Experimental investigation of a 500 W
584 traveling-wave thermoacoustic electricity generator. Chinese Science Bulletin.
585 2011;56:1975-7.
586 [20] Wu ZH, Zhang LM, Dai W, Luo EC. Investigation on a 1 kW traveling-wave
587 thermoacoustic electrical generator. Applied Energy. 2014;124:140-7.
588 [21] Wu ZH, Yu GY, Zhang LM, Dai W, Luo EC. Development of a 3 kW double-acting
589 thermoacoustic Stirling electric generator. Applied Energy (In press).
590 [22] Yu ZB, Jaworski AJ, Backhaus S. A low-cost electricity generator for rural areas
591 using a travelling-wave looped-tube thermoacoustic engine. Proceedings of the
592 Institution of Mechanical Engineers, Part A: Journal of Power and Energy.
593 2010;224:787-95.
594 [23] Yu ZB, Jaworski AJ, Backhaus S. Travelling-wave thermoacoustic electricity
595 generator using an ultra-compliant alternator for utilization of low-grade thermal energy.
596 Applied Energy. 2012;99:135-45.
597 [24] Kang H, Cheng P, Yu Z, Zheng H. A two-stage traveling-wave thermoacoustic

598 electric generator with loudspeakers as alternators. Applied Energy. 2015;137:9-17.
599 [25] Ward B, Clark J, Swift GW. Design Environment for Low-amplitude
600 Thermoacoustic Energy Conversion. Version 6.2. Users Guide.2008.
601 [26] Qiu LM, Wang B, Sun DM, Liu Y, Wang K. Study on energy flows in
602 thermoacoustic engines utilizing two-temperature heat sources. Energy Conversion and
603 Management. 2011;52:1066-72.
604 [27] Sun DM, Qiu LM, Wang B, Xiao Y, Zhao L. Output characteristics of Stirling
605 thermoacoustic engine. Energy Conversion and Management. 2008;49:1265-70.
606 [28] Hariharan NM, Sivashanmugam P, Kasthurirengan S. Influence of operational and
607 geometrical parameters on the performance of twin thermoacoustic prime mover.
608 International Journal of Heat and Mass Transfer. 2013;64:1183-8.
609 [29] http://www.qdrive.com/UI/SubCategoriesListing.aspx?cm=c1&mcid=115&pcid=1
610 15. Retrieved 19 Jan, 2015.
611
612